Improving the Single Point Positioning Accuracy in a Multi-Frequency Context with the Estimation of the Ionosphere delay

Clément Gazzino, Nicolas Lelarge, *Centre National d'Études Spatiales, Toulouse, France*
Alissa Kouraeva, Marion Laymand, *CS GROUP, Toulouse, France*

BIOGRAPHY

Clément Gazzino graduated from the French High Institute for Aeronautics and Space and obtained his master of engineering with a space systems specialisation. He obtained his PhD degree in space trajectory optimisation from the university of Toulouse. He is now working at the navigation department at CNES, the French space agency, and he is involved in the development of precise point positioning algorithms.

Nicolas Lelarge graduated from the French High Institute for Aeronautics and Space and obtained his master of engineering with a space systems specialisation. He is a member of the navigation system department at CNES, the French space agency, and he is involved in the development of precise point positioning algorithms.

Alissa Kouraeva graduated from the National School of Geographical Sciences in the Paris region with a specialisation in geodesy and positioning. She is currently working at CS GROUP as a navigation engineer and is involved in the development of GNSS algorithms for CNES.

Marion Laymand (PhD in astrophysics) is an engineer in the space business unit at CS GROUP. She is involved in the development of navigation algorithms for GNSS systems with CNES.

ABSTRACT

Classical methods for satellite navigation build ionosphere-free combination in order to remove the delays caused by the propagation of the signal in the atmosphere, and in particular the ionosphere. Since this signal combination has been set up in the early ages of the satellites navigation systems, it only uses two frequencies. This article proposes to explore ionosphere-free combinations with all the available frequencies. Such combinations always increase the observable noise. Therefore, an exploration of a Kalman filter estimating jointly the geometric and ionospheric parts of the observable models is performed. The results are applied in cases for low and high solar activities. As the new solar cycle begins, the ionospheric effects will be of importance for the years to come.

INTRODUCTION

The increasing number of Global Navigation Satellite Systems (GNSS) receivers around the world is an indicator of the widespread use of this positioning technology. Its principal interest lies in the fact that the localization is absolute, in contrast to other relative positioning techniques, like inertial positioning, for instance. Despite this main advantage, the GNSS technique suffers from error sources, in particular atmospheric delays. When the signal travels from the satellites to the ground through the ionosphere layer, composed of electrically charged particles, the code measurements suffer from a group velocity delay, and a phase velocity advance for carrier phase measurements (see Teunissen and Montenbruck (2017), Chen and Gao (2023) and the references therein).

Since the ionosphere is a dispersive propagation medium, using two frequencies in a so-called ionosphere-free combination effectively reduces the principal ionospheric effects, which often account for over 99% of the total ionospheric delay. This combination is equivalent to an instantaneous estimation of the ionosphere delay and its subtraction from the GNSS observable pseudorange and carrier-phase measurements. In this case, no dynamical model to take into account the slow variations of the ionosphere is used. Space weather strongly affects the Total Electron Content (TEC) in the ionosphere, and thus strongly impact the ionosphere delay seen from the receiver (see Jakowski et al. (2002) for instance).

The objective of the proposed paper is to enhance the positioning precision by estimating the ionosphere delay together with the geometry, especially in a multi-frequency context, taking advantage of the third and fourth frequencies of the GPS and Galileo constellations. To this end, we explicitly integrate the ionosphere delay term into both the conventional GNSS measurement and Kalman filter dynamical models. Special attention will be given in the biases datum in order to ensure a well-posed problem in a Kalman sense. The GNSS pseudorange (code) measurement model suffers from a rank deficiency since the clock offsets cannot be distinguished from the hardware biases. The State Space Representation (SSR) Format from the International GNSS Service

describes a solution to overcome this issue by the introduction of "Satellite Bias Datum" which sets the bias of certain signals or linear combinations of signals to zero (see International GNSS Service (2020)).

The method proposed in this paper explores the interest of going from a dual-frequency ionosphere-free combination to a minimal-noise multi-frequency one, and then the progress in estimating both the receiver position together with the ionosphere delay. This will be done in a Kalman filter, in order to take advantage of the slow variation of the ionosphere delay and its smoothing with the Doppler shift measurement. The proposed joint estimation of the receiver position together with the ionosphere delay and its drift is applied for the positioning of several ground station on Earth for several space weather conditions, with a high solar activity, and a low solar activity. Extension of this analysis will be performed to study the performances of a server generating GNSS orbit, clock, code and phase biases corrections as a function of the ionosphere elongation.

I GNSS ionospheric-free combination

1 GNSS measurements modeling

The pseudorange (code) and Doppler measurements from a GNSS satellite s at the frequency f_i (and wavelength λ_i) observed by a receiver r are modeled as (see Kaplan and Hegarty (2006)):

$$\begin{aligned} C_i &= \rho_r^s + h_r^s + \gamma_i e^s + m(E^s)T_z + b_{r,C_i}^s, \\ D_i &= -\lambda_i \Delta f_i = \dot{\rho_r^s} + \dot{h}_r^s - \gamma_i \dot{e}^s + b_{r,D_i}^s, \end{aligned} \tag{1}$$

where C_i is the code measurement expressed in the unit of distance, and D_i is the equivalent Doppler shift measurement expressed in the unit of distance per time. The quantities $h_r^s = h_r - h^s$ is the clock offset between the satellite and the receiver, e^s is the slant ionospheric delay at the reference frequency $f_1 = 1575.42$ MHz (corresponding to the L1 / E1 signals) for the satellite s, $\gamma_i = f_1^2/f_i^2$ and T_z is the zenithal wet tropospheric delay, $m(E^s)$ is the mapping function depending on the satellite elevation E^s of the satellite s. ρ_r^s is the geometric distance between the satellite s and the receiver r including the phase center offset correction. The difference between the sofware and hardware code biases at the satellite and receiver levels on the frequency f_i is denoted $b_{r,C_i}^s = b_{r,C_i} - b_{C_i}^s$.

The Doppler shift measurement Δf_i is the difference between the observed and emitted frequency of the carrier; its sign is usually defined positive for approaching satellites. To make the equations simpler, phenomena like the Shapiro effect, Sagnac effect, phase center offset and zenithal dry tropospheric delay were removed from the measurements and supposed to be already taken into account. $b_{r,D_i}^s = b_{r,D_i} - b_{D_i}^s$ accounts for a frequency bias on the signals between the satellite s and the receiver r that can be caused by a clock drift, as modeled in Gioia et al. (2023) and the references therein. This bias is frequency dependent (see for instance Wang et al. (2023)).

The undifferenced satellite code biases, as well as the satellite part of the clock offset, are retrieved from existing products. In our case they are recovered as Observable Specific Biases (OSB) from the ones computed by the PPP-WIZARD demonstrator as described in the reference Laurichesse (2011). The satellite part of the Doppler bias is likewise compensated by the information retrieved from the navigation message, so that only the receiver part remains to be estimated (see Gioia et al. (2023). The code and Doppler model equations (1) are thus modified to remove the already known components from the right-hand side. With these definitions, the code and phase measurement models at the frequency f_i are rewritten as:

$$\begin{aligned} \tilde{C}_i &= C_i + h^s + b_{C_i}^s = \rho_r^s + h_r + b_{r,C_i} + \gamma_i e^s + m(E^s)T_z \\ \tilde{D}_i &= D_i + \dot{h}_s + b_{D_i}^s = \dot{\rho_r^s} + \dot{h}_r - \gamma_i \dot{e}^s. \end{aligned} \tag{2}$$

Multipath delay is not taken into account in this model, and lies in the observation noise. For readability reasons, the tilda superscript of the receiver observables will be removed throughout the remainder of the article.

The navigation equations (2) are generally linearized around an initial guess of the receiver position and velocity or a around a reference position/velocity in the case of a reference station. The equations (2) are thus rewritten as:

$$\begin{aligned} \Delta\tilde{C}_i &= \mathbf{u}_r^s \cdot \Delta\mathbf{p}_r + h_r + b_{r,C_i} + \gamma_i e^s + m(E^s)T_z \\ \Delta\tilde{D}_i &= \mathbf{u}_r^s \cdot \Delta\mathbf{v}_r + \dot{h}_r - \gamma_i \dot{e}^s, \end{aligned} \tag{3}$$

where $\Delta\tilde{C}_i$ and $\Delta\tilde{D}_i$ are respectively the residuals code and Doppler measurements with respect to the one at the reference receiver position/velocity. $\Delta\mathbf{p}_r$ and $\Delta\mathbf{v}_r$ are the position and velocity increment with respect to the reference. $\mathbf{u}_r^s$ is the unit vector from the receiver to the satellite s in row form.

2 Bias datum

The IGS-SSR standards International GNSS Service (2020) emphasizes the fact that the observation problem defined by the equation (3) is rank-deficient. The same analysis has been performed by the reference Odijk et al. (2016). In order to overcome this deficiency, the solution is to define a bias datum, meaning that the bias of a certain signal or linear combination of signals is set to zero.

In a dual frequency case, this leads to the well-known Interfrequency Biases (ISB). They are defined in the following way. The receiver code biases b_{r,C_i} and b_{r,C_j} for the pseudorange measures at frequencies f_i and f_j are broken down into a iono-free (IF) bias and a geometry-free (GF) bias:

$$\begin{aligned} b_{r,C_i} &= b_{r,\text{IF},ij} + \gamma_i b_{r,\text{GF},ij}, \\ b_{r,C_j} &= b_{r,\text{IF},ij} + \gamma_j b_{r,\text{GF},ij}, \end{aligned} \tag{4}$$

with the dual frequency IF bias being defined as $b_{r,\text{IF},ij} = \frac{\gamma_j b_{r,C_i} - \gamma_i b_{r,C_j}}{\gamma_j - \gamma_i}$, and the dual-frequency GF bias as $b_{r,\text{GF},ij} = \frac{b_{r,C_i} - b_{r,C_j}}{\gamma_i - \gamma_j}$.

I n the dual frequency case, the code observation model given by the Equation (3) is transformed with such a decomposition to:

$$\begin{aligned} C_i &= \mathbf{u}_r^s \cdot \Delta\mathbf{p}_r + h_r + b_{r,\text{IF},ij} + m(E^s)T_z + \gamma_i(e^s + b_{r,\text{GF},ij}), \\ C_j &= \mathbf{u}_r^s \cdot \Delta\mathbf{p}_r + h_r + b_{r,\text{IF},ij} + m(E^s)T_z + \gamma_j(e^s + b_{r,\text{GF},ij}). \end{aligned} \tag{5}$$

Classical methods in navigation remove the ionosphere delay by forming the ionosphere-free combination, see for instance (Teunissen and Montenbruck, 2017, Chapter 20). Building the IF combination of these two code measurements leads to:

$$C_{\text{IF},ij} = \mathbf{u}_r^s \cdot \Delta\mathbf{p}_r + h_r + b_{r,\text{IF},ij} + m(E^s)T_z. \tag{6}$$

As a consequence, the datum described in the IGS-SSR format takes the form of the dual frequency ionosphere receiver clock $h_{r,\text{IF},ij} = h_r + b_{r,\text{IF},ij}$, which is the receiver counterpart of the ionosphere satellite clock broadcast in the navigation message or retrieved from precise products. Hence, the rank deficiency is reduced by 1 and the full-rank code observation models reads:

$$C_{\text{IF},ij} = \mathbf{u}_r^s \cdot \Delta\mathbf{p}_r + h_{r,\text{IF},ij} + m(E^s)T_z. \tag{7}$$

If the ionosphere delay is not removed by a IF combination, another rank deficiency of the observation model remains, since both the ionosphere delay e^s and the GF code bias $b_{r,\text{GF},ij}$ cannot be estimated independently. Therefore, the resolution of the second rank deficiency consists in the estimation of a biased ionospheric delay:

$$e^s_{r,\text{GF},ij} = e^s + b_{r,\text{GF},ij}, \tag{8}$$

and the full-rank code observation model with ionosphere delay reads:

$$C_i = \mathbf{u}_r^s \cdot \Delta\mathbf{p}_r + h_{r,\text{IF},ij} + m(E^s)T_z + \gamma_i e^s_{r,\text{GF},ij}. \tag{9}$$

The transformation presented in this section solve for the rank deficiency of the code observation model, and match the IGS-SSR format recommendation of removing two biases when estimating the ionosphere delay.

The satellite navigation systems provide now signals on more than two frequencies. The previously introduced IF clock and biased ionosphere delay have thus to be integrated in the code observation model of the new frequency. Let f_k denote a third frequency broadcast by the considered GNSS. Its code observation model is transformed in the following way:

$$\begin{aligned} C_k &= \mathbf{u}_r^s \cdot \Delta\mathbf{p}_r + h_r + m(E^s)T_z + \gamma_k e^s + b_{r,C_k}, \\ &= \mathbf{u}_r^s \cdot \Delta\mathbf{p}_r + h_{r,\text{IF},ij} + m(E^s)T_z + \gamma_k e^s_{r,\text{GF},ij} + b_{r,C_k,\text{IF}_{ij}}, \end{aligned} \tag{10}$$

with $b_{r,C_k,\text{IF}_{ij}}$ the code bias on the frequency f_k defined with respect to the IF and GF biases of the two frequencies f_i and f_j as:

$$b_{r,C_k,\text{IF}_{ij}} = b_{r,C_k} - b_{r,\text{IF},ij} - \gamma_k b_{r,\text{GF},ij}. \tag{11}$$

Similarly as for the code model, the Doppler model is rank deficient. Building the IF Doppler combination leads to:

$$D_{\text{IF},ij} = \mathbf{u}_r^s \cdot \Delta\mathbf{v}_r + \dot{h}_r + \frac{\gamma_j b_{r,D_i} - \gamma_i b_{r,D_j}}{\gamma_j - \gamma_i}. \tag{12}$$

Defining the Doppler bias datum with the IF clock drift as:

$$\dot{h}_{r,\text{IF},ij} = \dot{h}_r + \frac{\gamma_j b_{r,D_i} - \gamma_i b_{r,D_j}}{\gamma_j - \gamma_i}, \tag{13}$$

removes the rank deficiency. The IF Doppler model thus reads:

$$D_{\text{IF},i} = \mathbf{u}_r^s \cdot \Delta\mathbf{v}_r + \dot{h}_{r,\text{IF},ij}. \tag{14}$$

In the case where the ionosphere drift delay is kept in the Doppler observation model, it possible to define a new clock drift parameter absorbing the Doppler bias of the first frequency, with $\dot{h}_{r,i} = \dot{h}_r + b_{r,D_i}$. As a consequence, the Doppler biases of the other frequencies must be defined with the respect to the one of the first frequency: $b_{r,D_j,i} = b_{r,D_j} - b_{r,D_i}$. The modified Doppler model is thus recast as:

$$\begin{aligned} D_i &= \mathbf{u}_r^s \cdot \Delta\mathbf{v}_r + \dot{h}_{r,i} - \gamma_i \dot{e}^s, \\ D_{j\neq i} &= \mathbf{u}_r^s \cdot \Delta\mathbf{v}_r + \dot{h}_{r,i} - \gamma_j \dot{e}^s + b_{r,D_j,i}. \end{aligned} \tag{15}$$

II Ionosphere-free Single Point Positioning Solutions

1 Positioning in a Dual-Frequency Framework

The GNSS signals are broadcast on at least two frequencies for all the constellations, with the exception of GLONASS that relies on the Frequency-Division Multiple Access (FDMA) technique. Since the ionosphere is a dispersive medium, the signal delay depends on its carrier frequency. This delay term can be cancelled out by combining the observables gathered at the two frequencies, resulting in the so-called Dual Frequency (DF) Ionosphere-free (IF) code and Doppler combinations:

$$\begin{aligned} C_{ij}^{\text{IF}} &= \mathbf{u}_r^s \cdot \Delta\mathbf{p}_r + h_{r,\text{IF}_{ij}} + m(E^s)T_z, \\ D_{ij}^{\text{IF}} &= \mathbf{u}_r^s \cdot \Delta\mathbf{v}_r + \dot{h}_r^s, \end{aligned} \tag{16}$$

with $b_{r,D,\text{IF},ij}$ the IF Doppler receiver bias. The following developments assume that the code and Doppler measurements at one frequency are not correlated with those at another frequency. Using this hypothesis, if the standard deviation of the code and Doppler measurements are written σ_C and σ_D respectively, the standard deviation of a IF combination is computed as follows:

$$\sigma_{C,\text{IF},ij} = \frac{\sqrt{\gamma_i^2 + \gamma_j^2}}{|\gamma_i - \gamma_j|}\sigma_C, \qquad \sigma_{D,\text{IF},ij} = \frac{\sqrt{\gamma_i^2 + \gamma_j^2}}{|\gamma_i - \gamma_j|}\sigma_D. \tag{17}$$

It can be noticed that the noise amplification coefficient is greater than one, with the lowest value obtained for the combination with the most separated frequencies. The Table 1 shows the increase of the noise level due to this combination. The code standard deviations for the Galileo and GPS constellations have been assumed to be 0.5 m and 1 m respectively. The Doppler standard deviations for both have been assumed to be 0.15 m/s. These values will be employed throughout this article for the theoretical noise analysis.

Combination DF-IF ij	E5a-E5b	E6-E5a	E6-E5b	E5a-E1	E5b-E1	E6-E1
$\sigma_{C,\text{IF}-\text{DF},ij}$ [m]	13.736	4.265	6.152	1.294	1.404	1.755
$\sigma_{D,\text{IF}-\text{DF},ij}$ [m/s]	4.121	1.279	1.846	0.388	0.421	0.527

(a) Galileo

Combination DF-IFij	L1-L2	L1-L5	L2-L5
$\sigma_{C,\text{DF}-\text{IF},ij}$ [m]	2.186	1.783	9.665
$\sigma_{D,\text{DF}-\text{IF},ij}$ [m/s]	0.328	0.267	1.450

(b) GPS

Table 1: Standard deviation of the noise for the DF-IF combination for Galileo and GPS

The receiver position is estimated with a Kalman filter. Its state vector is made of the receiver position, its velocity, the receiver clock offset, the receiver clock drift, the wet zenithal troposphere delay and the receiver Doppler hardware biases as well as the

troposphere delay:

$$X = \begin{bmatrix} \Delta p_r^T & \Delta v_r^T & h_{r,\text{IF},ij} & \dot{h}_{r,\text{IF},ij} & T_z \end{bmatrix}^T \tag{18}$$

The prediction phase of the Kalman filter links the position and velocity estimated a the epoch k to the ones at the epochs $k+1$ with a first order explicit Euler scheme and the other elements of the state vector are supposed to remain constant. The state transition matrix thus reads:

$$A = \begin{bmatrix} I_3 & \Delta t\, I_3 & 0_3 \\ 0_3 & I_3 & 0_3 \\ 0_3 & 0_3 & I_3 \end{bmatrix}, \tag{19}$$

such that $X(k+1) = AX(k)$. Δt is the time interval between the epochs k and $k+1$, I_n is the identity matrix of dimension n, and 0_n is the zero matrix of dimension n.

2 Positioning in a Multi-Frequency Framework

Most of the navigation satellites provide measurements on more than two frequencies. Classical methods only pick up two of the available frequencies to build an IF combination. That is what is done for instance with the Galileo F/NAV navigation message (E1-E5a dual frequency combination) or I/NAV (E1-E5b dual frequency combination) that broadcast IF clocks and Broadcast Group Delays (BGD) for a dual frequency combination. Nevertheless, it is possible to build an IF combination that takes advantage of all the provided frequencies. This enables the construction of a new Multi Frequency (MF) IF linear combination:

$$C_{\text{IF},1,\ldots,n} = \sum_{i=1}^{n} \alpha_i C_i \quad \text{and } D_{\text{IF},1,\ldots,n} = \sum_{i=1}^{n} \alpha_i D_i. \tag{20}$$

In order to build a IF combination, two constraints have to be applied on the α_i coefficients. If more than two frequencies are available, there are more degrees of freedom than constraints to be applied. Therefore, the parameters can be chosen in order to minimize a given objective function, for instance the noise of the combination. The α_i are thus solutions of the following minimization problem:

$$\min_{\alpha_i, i=1,\ldots,n} \sum_{i=1}^{n} \alpha_i^2, \quad \text{such that } \begin{cases} \sum\limits_{i=1}^{n} \alpha_i = 1, \\ \sum\limits_{i=1}^{n} \alpha_i \gamma_i = 0. \end{cases} \tag{21}$$

This is an under-determined least-squares problem whose solution is given by:

$$\alpha_i = \frac{\sum\limits_{j=1}^{n} \gamma_j^2 - \gamma_i \left(\sum\limits_{j=1}^{n} \gamma_j \right)}{n \sum\limits_{j=1}^{n} \gamma_j^2 - \left(\sum\limits_{j=1}^{n} \gamma_j \right)^2}. \tag{22}$$

The numerical values of the coefficients for the GPS and Galileo constellations, as well as the expected noise level for the code and the Doppler measures are given in the Table 2. Note that in a dual frequency case, the classical IF combination is found.

We can observe in the Table 2a for the Galileo constellation that considering the MF-IF combination of the four code measurements does not bring improvement compared to the use of the combination with the three frequencies E1, E5a and E5b. In contrast, the three-frequency solution for both constellation is better than the dual frequency, with a reduction in noise of almost 5%.

The proposed MF IF combination prevents from using the broadcast BGD in order to remove the satellite part of the code hardware biases. They are indeed built together with the IF clock so that they vanish when applied within a DF IF combination. In the case of a MF IF combination, Observable Specific Biases (OSB) have to be used.

Following the rank deficiency resolution process described in the Section I.2, the development of the MF-IF combination with the code observation models (9) and (10) with more than three frequencies leads to:

$$C_{\text{IF},1,\ldots,n} = \sum_{i=1}^{n} \alpha_i C_i, \; = \mathbf{u}_r^s \cdot \Delta \mathbf{p}_r + h_{r,\text{IF},ij} + m(E^s) T_z + \sum_{k=3}^{n} b_{r,C_k,\text{IF}_{12}}. \tag{23}$$

E1	E5a	E5b	E6	$\|\alpha\|^2$	$\sigma_{C_{\text{IF}}}\,[m]$	$\sigma_{D_{\text{IF}}}\,[m/s]$
2.261	−1.261			6.699	1.294	0.388
2.422		−1.422		7.888	1.404	0.421
2.931			−1.931	12.321	1.755	0.527
	−18.920	19.920		754.764	13.736	4.121
	−5.510		6.510	72.750	4.265	1.279
		−8.186	9.186	151.385	6.152	1.846
2.315	−0.836	−0.479		6.287	1.254	0.376
2.269	−1.245		−0.025	6.699	1.294	0.388
2.489		−1.235	−0.253	7.784	1.395	0.419
	−4.828	−1.014	6.842	71.147	4.217	1.265
2.255	−0.904	−0.545	0.193	6.237	1.249	0.375

(a) Galileo

L1	L2	L5	$\|\alpha\|^2$	$\sigma_{C_{\text{IF}}}\,[m]$	$\sigma_{D_{\text{IF}}}\,[m/s]$
2.546	−1.546		8.870	2.978	0.447
2.261		−1.261	6.699	2.588	0.388
	12.255	−11.255	276.875	16.640	2.496
2.327	−0.360	−0.967	6.480	2.546	0.382

(b) GPS

Table 2: Coefficients and noise amplification of the noise-optimal MF-IF combinations with three or more frequencies.

The Equation (23) is rank-deficient because of the code bias of the third to n^{th} frequencies. The deficiency can be solved while including the sum of the code biases into the receiver clock offset defining:

$$h_{r,\text{MF-IF},12} = h_{r,\text{IF},12} + \sum_{k=3}^{n} b_{r,C_k,\text{IF}_{12}}. \tag{24}$$

Similarly, the development of the MF-IF Doppler model (15) with more than two frequencies leads to:

$$D_{\text{IF},1,\ldots,n} = \sum_{i=1}^{n} \alpha_i D_i, \; = \mathbf{u}_r^s \cdot \Delta\mathbf{v}_r + \dot{h}_{r,1} + \sum_{k=2}^{n} b_{r,D_k,1}. \tag{25}$$

The Equation (25) is rank deficient because of the Doppler bias of the second to n^{th} frequencies. The deficiency can be solved while including the sum of the Doppler biases into the receiver clock drift defining:

$$\dot{h}_{r,\text{MF-IF},1} = \dot{h}_{r,1} + \sum_{k=2}^{n} b_{r,D_k,1}. \tag{26}$$

The Doppler biases are already absorbed in the receiver clock drift, as shown in the Equation (14). The receiver position is estimated with a Kalman filter in the same way as in the dual-frequency context.

III Single Point Positioning with Ionospheric delay Estimation

It has been shown that using an ionosphere-free combination leads to an increase of the observable noise level with respect to the single original code and Doppler signals. Nevertheless, it is also possible to employ uncombined observables for the estimation of the receiver position. In this case, the ionospheric delay of each visible satellite will be determined jointly with the receiver position and velocity. Since the ionosphere drift also appears in the Doppler observable model, it will be estimated together with the receiver velocity. The state vector of the IF case defined in the Equation (18) has thus to be enhanced to incorporate the slant ionosphere delays and drifts of the GNSS satellites in visibility of the receiver.

According to the Section I.2, code and Doppler biases have to be taken into account in the models. In the case in which more than two code signals are received, it is mandatory to add in the state vector a bias term for each acquired signal on top of the

third frequency. Similarly, if more than one Doppler shift is received, one Doppler bias will be added in the state vector on top of the second frequency.

Assuming that n_S satellites are visible from the receiver and that n_f frequencies are transmitted from these satellites, the new state vector reads:

$$X = \begin{bmatrix} \Delta p_r^T & \Delta v_r^T & e^1_{\text{GF},12} & \cdots & e^{n_S}_{\text{GF},12} & \dot{e}^1 & \cdots & \dot{e}^{n_S} & h_{r,\text{IF},ij} & \dot{h}_{r,i} & T_z & b_{r,C_3,\text{IF}_{12}} & b_{r,C_{n_f},\text{IF}_{12}} & b_{r,D_2,\text{IF}_{12}} & b_{r,C_{n_f},\text{IF}_{12}} \end{bmatrix}^T. \tag{27}$$

Although the state vector of the IF problem only has 9 components, the state vector for the ionosphere and geometry estimation problem has $n_K = 9 + 2n_S + 2n_f - 3$ components, with the assumption that the signals from the GNSS satellites are transmitted on at least two frequencies.

For each satellite, the prediction phase of the Kalman filter links the ionosphere delay and its drift with a first order explicit Euler scheme. However, as seen in the Section I.2, the ionosphere delay involved in the code observable is biased with the GF combination of the code bias of the two first frequencies. Considering the time variations of b_{r,C_i} and b_{r,C_j} negligible compared to the variations of e^s, $\dot{e}^s_{\text{GF},ij} \approx \dot{e}^s$. The predicted ionosphere delay and drift at time k are thus:

$$\forall s,\ \begin{bmatrix} e^s_{\text{GF},ij}(k) \\ \dot{e}^s(k) \end{bmatrix} = \begin{bmatrix} 1 & \Delta t \\ 0 & 1 \end{bmatrix} \begin{bmatrix} e^s_{\text{GF},ij}(k-1) \\ \dot{e}^s(k-1) \end{bmatrix} + \begin{bmatrix} \varpi_e(k) \\ \varpi_{\dot{e}}(k) \end{bmatrix} \tag{28}$$

with ϖ_e and $\varpi\dot{e}$ the process noise for the ionosphere delay and its drift respectively. The clock offset, the clock drift and the biases are assumed to have a random walk evolution, whose process noise has to be chosen. The state prediction matrix for the whole state vector is thus:

$$A = \begin{bmatrix} I_3 & \Delta t\, I_3 & 0_{3\times n_S} & 0_{3\times n_S} & 0_{3\times(2n_f-3)} \\ 0_3 & I_3 & 0_{3\times n_S} & 0_{3\times(2n_f-3)} & \\ 0_3 & 0_3 & I_{n_S} & \Delta t\, I_{n_S} & 0_{n_S\times(2n_f-3)} \\ 0_3 & 0_3 & 0_{n_S} & I_{n_S} & 0_{n_S\times(2n_f-3)} \\ 0_3 & 0_3 & 0_{(2n_f-3)\times n_S} & 0_{(2n_f-3)\times n_S} & I_{2n_f-3} \end{bmatrix}. \tag{29}$$

Let G^s be the matrix that stacks the unit vectors towards all the n_S visible satellites, and $\mathbf{m}^s$ the mapping functions vector of all the satellites. The observables are stacked in a measurement vector: for each frequency, the code observables of all the satellites are gathered together and added to the measurement vector. After that, the Doppler observables of all the satellites are gathered together and added to the measurement vector. The measure matrix of the Kalman filter H thus reads:

$$H = \begin{bmatrix} G^s & 0 & \gamma_1 I & 0 & \mathbf{1} & 0 & \mathbf{m}^s & 0 & \cdots & 0 & 0 & \cdots & 0 \\ \vdots & \vdots & \gamma_2 I & \vdots & \vdots & \vdots & \vdots & 0 & \cdots & 0 & \vdots & & \vdots \\ \vdots & & \gamma_3 I & & & & & \mathbf{1} & & & & & \\ \vdots & \vdots & \vdots & \vdots & \vdots & \vdots & \vdots & & \ddots & & \vdots & & \vdots \\ G^s & 0 & \gamma_{n_f} I & 0 & 1 & 0 & \mathbf{m}^s & & & \mathbf{1} & 0 & \cdots & 0 \\ 0 & G^s & 0 & -\gamma_1 I & 0 & \mathbf{1} & 0 & 0 & \cdots & 0 & 0 & \cdots & 0 \\ \vdots & \vdots & \vdots & -\gamma_2 I & \vdots & \vdots & \vdots & \vdots & & \vdots & \mathbf{1} & & \\ \vdots & \vdots & \vdots & \vdots & \vdots & \vdots & \vdots & \vdots & & \vdots & & \ddots & \\ 0 & G^s & 0 & -\gamma_{n_f} I & 0 & 1 & 0 & 0 & \cdots & 0 & & & \mathbf{1} \end{bmatrix}. \tag{30}$$

With the provided process and observation matrices A and H, the system is fully observable. This can be verified computing the rank of the Kalman observability matrix (see Jazwinski (2007) for instance). The system is observable if the observability matrix defined by:

$$\mathcal{O} = \begin{bmatrix} A \\ HA \\ \vdots \\ HA^{n_K-1} \end{bmatrix}, \tag{31}$$

has rank n_K.

For a given $i \in \mathbb{N}$, the matrix HA^i is computed as:

$$HA^i = \begin{bmatrix} G^s & i\Delta t\, G^s & \gamma_1\, I & i\Delta t\gamma_1\, I & \mathbf{1} & 0 & \mathbf{m}^s & 0 & \cdots & 0 & 0 & \cdots & 0 \\ \vdots & \vdots & \gamma_2\, I & i\Delta t\gamma_2\, I & \vdots & \vdots & \vdots & 0 & \cdots & 0 & \vdots & & \vdots \\ \vdots & & \gamma_3\, I & i\Delta t\gamma_3\, I & & & & \mathbf{1} & & & & & \\ \vdots & \vdots & \vdots & \vdots & \vdots & \vdots & \vdots & & \ddots & & \vdots & & \vdots \\ G^s & i\Delta t\, G^s & \gamma_{n_f}\, I & i\Delta t\gamma_{n_f}\, I & \mathbf{1} & 0 & \mathbf{m}^s & & & 1 & 0 & \cdots & 0 \\ 0 & G^s & 0 & -\gamma_1\, I & 0 & \mathbf{1} & 0 & 0 & \cdots & 0 & 0 & \cdots & 0 \\ \vdots & \vdots & \vdots & -\gamma_2\, I & \vdots & \vdots & \vdots & \vdots & & \vdots & \mathbf{1} & & \\ \vdots & \vdots & \vdots & \vdots & \vdots & \vdots & \vdots & \vdots & & \vdots & & \ddots & \\ 0 & G^s & 0 & -\gamma_{n_f}\, I & 0 & \mathbf{1} & 0 & 0 & \cdots & 0 & & & \mathbf{1} \end{bmatrix}. \tag{32}$$

Concatenating all the HA^i matrices, and applying linear combinations on rows and columns on the observability matrix $\mathcal{O}$, the rank of $\mathcal{O}$ is equal to the rank of the matrix:

$$\begin{bmatrix} G^s & \mathbf{m}^s & \mathbf{1} & \gamma_1 I & 0 & 0 & 0 & 0 & \cdots & 0 & 0 & \cdots & 0 \\ 0 & 0 & 0 & (\gamma_2-\gamma_1)I & 0 & 0 & 0 & 0 & \cdots & 0 & 0 & \cdots & 0 \\ 0 & 0 & 0 & 0 & G^s\Delta t & \gamma_1\Delta t\, I & 0 & 0 & \cdots & 0 & 0 & \cdots & 0 \\ 0 & 0 & 0 & 0 & 0 & (\gamma_2-\gamma_1)\Delta t\, I & 0 & 0 & \cdots & 0 & 0 & \cdots & 0 \\ 0 & 0 & 0 & 0 & 0 & 0 & \Delta t & 0 & \cdots & 0 & 0 & \cdots & 0 \\ 0 & 0 & 0 & 0 & 0 & 0 & 0 & (\gamma_2-\gamma_1)\mathbf{1} & & & 0 & \cdots & 0 \\ 0 & 0 & 0 & 0 & 0 & 0 & 0 & 0 & \ddots & & 0 & \cdots & 0 \\ 0 & 0 & 0 & 0 & 0 & 0 & 0 & 0 & & (\gamma_2-\gamma_1)\mathbf{1} & 0 & \cdots & 0 \\ 0 & 0 & 0 & 0 & 0 & 0 & 0 & 0 & \cdots & 0 & \Delta t & & \\ 0 & 0 & 0 & 0 & 0 & 0 & 0 & 0 & \cdots & 0 & & (\gamma_2-\gamma_1)\mathbf{1} & \\ 0 & 0 & 0 & 0 & 0 & 0 & 0 & 0 & \cdots & 0 & & & (\gamma_2-\gamma_1)\mathbf{1} \end{bmatrix}. \tag{33}$$

This matrix is in block triangular form. As the satellites are assumed to be at different locations in the sky, the G^s matrix has full rank. It follows that the matrix of the Equation (33) has a rank equal to $9 + 2n_S + 2n_f - 3$, which is exactly the number of states. This enhances the results given by the reference Odijk et al. (2016), since the proposed model takes advantage of the Doppler measurements.

IV Positioning results

This section evaluates the described positioning technique by the joint estimation of the geometry and the ionosphere delay. The study was conducted on data from three different ground stations: one near the equator (KOUG), one at mid latitudes (TLSE), and one near a pole (METG, near the North Pole). For each station several dates were selected in order to observe the impact of the solar activity on the ionospheric delay: December 1st, 2023 – DOY 2023-335, December 11th, 2023 – DOY 2023-345, and May, 11th, 2024 – DOY 2024-132. On each of these dates, the solar activity could be evaluated through the Kp index. The values of this index is summarized in the Table 3. The day 2023-345 was a day with a very low activity, for which Kp was equal to 1. The days 2023-335 and 2023-113 were days with a medium solar activity with Kp equal to 7 and 8 respectively, and the day 2024-132 was a very active day in a geomagnetic point of view, since the Kp index reached 11. The influence of the solar eruption was expected to be seen in the computed results.

DOY	2023-335	2023-345	2024-132
Kp index	7	1	11

Table 3: Kp index for the selected days.

The computed positions for each station were compared to the reference coordinates in ITRF given by the REGINA service at that date. The map of the Figure 1 displays the geographic spread of the selected stations.

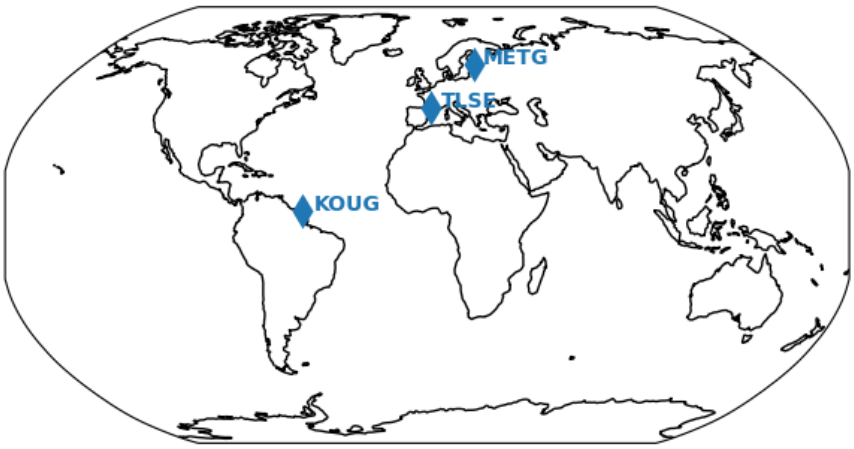

Figure 1: Map of the three stations used for the study: KOUG near the equator, TLSE at mid-latitude, and MET3 near the North Pole.

Each of the described and implemented methods required a fine tuning of the different Kalman filter parameters, in particular the process noise standard deviation. More than 20 configurations were tested and four were selected as best for comparison. Table 4 shows the different configurations with the value of the changed parameters. Configuration 1 was used as the nominal configuration to allow comparison. The process noises that were not changed throughout the analysis are presented on the Table 5.

Configuration	$\Delta \mathbf{v}_r$ [m/s]	e^s [m]	$\dot{e}^s$ [m/s]
1 (nominal)	$[0.05,\ 0.05,\ 0.05]$	0.1	0.1
2	$[1.0,\ 1.0,\ 1.0]$	0.1	0.1
3	$[0.05,\ 0.05,\ 0.05]$	1.0	0.1
4	$[0.05,\ 0.05,\ 0.05]$	0.1	1.0

Table 4: Process noise standard deviations changed for each configuration. Configuration 1 is assumed to be the nominal one.

Parameter	Standard deviation
Position	[0.0, 0.0, 0.0] m
Clock	10^5 m
Clock drift	10^{-3} m/s
Biased	10^{-3} m
Troposphere	1 m

Table 5: Process noise standard deviations unchanged throughout all the configurations.

The Tables 6, 7 and 8 gives the position estimation errors in the station local East, North, Up coordinate frame for the DOY 2023-335, 2023-345, and 204-132 respectively. These Tables demonstrate that the positioning errors highly depends on the settings of the Kalman filters, as it could be expected. On top of that, both the Kp index of the considered day and the location of the ground station on the Earth play a significant role in the positioning accuracy. For the day with a very low solar activity, the joint estimation of the position and the ionospheric delay decreases the positioning errors only for the station located near the Equator. This is explained by the fact that the station is located under the ionosphere bulge, whereas the other ones are higher in latitude, so that the ionospheric estimation do not brings improvement. Therefore estimating the ionosphere delay together with the ionosphere helps mitigating the disturbing effects. For the station located at the pole, the configuration with a high velocity noise leads to an increase of the positioning accuracy. On the Figure 2 displaying the positioning errors of the KOUG station for the low solar activity day, the ionosphere-free combination does not remove all the ionosphere delay. An estimation of this delay is therefore mandatory in order to improve the positioning accuracy. Such an improvement in the positioning accuracy can also be seen on the KOUG station for the medium solar activity case. In such a situation, the positioning at the METG station near the poles is also increased for a special set of the configuration parameters.

For high Kp indexes, the results are opposite to the one obtained for low Kp indexes. The estimation of the position near the poles is enhanced by the joint estimation of the ionosphere whereas for lower latitude, the chosen values for the configuration

		KOUG			TLSE			METG		
		E [m]	N [m]	U [m]	E [m]	N [m]	U [m]	E [m]	N [m]	U
Ionofree	Conf. 1	0.34	0.304	1.935	0.216	0.32	2.241	0.175	0.232	1.962
	Conf. 2	0.336	0.302	0.916	0.215	0.318	2.234	0.184	0.259	2.004
	Conf. 3	0.34	0.304	1.935	0.216	0.32	2.241	0.175	0.232	1.962
	Conf. 4	0.34	0.304	1.935	0.216	0.32	2.241	0.175	0.232	1.962
Geometry and iono estimation	Conf. 1	0.297	0.227	1.522	0.397	0.426	2.335	0.197	0.306	1.63
	Conf. 2	0.296	0.226	1.5	0.397	0.419	2.401	0.201	0.336	1.712
	Conf. 3	0.304	0.232	0.576	0.4	0.423	2.45	0.158	0.352	1.19
	Conf. 4	0.297	0.223	1.527	0.397	0.418	2.417	0.174	0.337	1.355

Table 6: RMS results for different configurations for 01/12/2023 (DOY 2023-335), with a Kp index equal to 7. Results are computed for in East (E), North (N) and Up (U) directions in meters.

		KOUG			TLSE			METG		
		E [m]	N [m]	U [m]	E [m]	N [m]	U [m]	E [m]	N [m]	U
Ionofree	Conf. 1	0.328	0.28	1.67	0.336	0.413	2.712	0.259	0.363	3.002
	Conf. 2	0.349	0.292	1.681	0.351	0.43	2.72	0.263	0.373	2.958
	Conf. 3	0.328	0.28	1.67	0.366	0.413	2.712	0.256	0.357	2.959
	Conf. 4	0.328	0.28	1.67	0.366	0.413	2.712	0.256	0.357	2.959
Geometry and iono estimation	Conf. 1	0.277	0.212	1.125	0.498	0.844	4.457	0.319	0.64	3.709
	Conf. 2	0.308	0.233	1.155	0.506	0.866	4.477	0.165	0.244	0.783
	Conf. 3	0.277	0.212	1.125	0.498	0.844	4.457	0.319	0.64	3.709
	Conf. 4	0.275	0.21	1.125	0.504	0.854	4.5	0.318	0.638	3.703

Table 7: RMS results for different configurations for 11/12/2023 (DOY 2023-345), with a Kp index equal to 1. Results are computed for in East (E), North (N) and Up (U) directions in meters.

parameters prevents from obtaining good positioning results. The Figure 3 shows the fact that for high solar activities the higher order ionospheric effects have to be taken into account, and the classically used ionosphere-free is not sufficient enough.

		KOUG			TLSE			METG		
		E [m]	N [m]	U [m]	E [m]	N [m]	U [m]	E [m]	N [m]	U
Ionofree	Conf. 1	0.305	0.233	1.979	0.288	0.418	2.093	0.241	0.308	1.837
	Conf. 2	0.324	0.249	1.994	0.302	0.435	2.108	0.261	0.336	1.839
	Conf. 3	0.305	0.233	1.979	0.288	0.418	2.093	0.252	0.319	1.83
	Conf. 4	0.305	0.233	1.979	0.288	0.418	2.093	0.252	0.319	1.83
Geometry and iono estimation	Conf. 1	0.62	0.802	4.242	0.512	0.796	4.798	0.151	0.21	0.694
	Conf. 2	0.633	0.806	4.423	0.525	0.806	4.478	0.443	0.679	2.915
	Conf. 3	0.619	0.802	4.422	0.515	0.811	4.8	0.151	0.21	0.694
	Conf. 4	0.619	0.801	4.424	0.512	0.794	4.806	0.429	0.663	2.898

Table 8: RMS results for different configurations for 11/05/2024 (DOY 2024-132), with a Kp index equal to 11. Results are computed for in East (E), North (N) and Up (U) directions in meters.

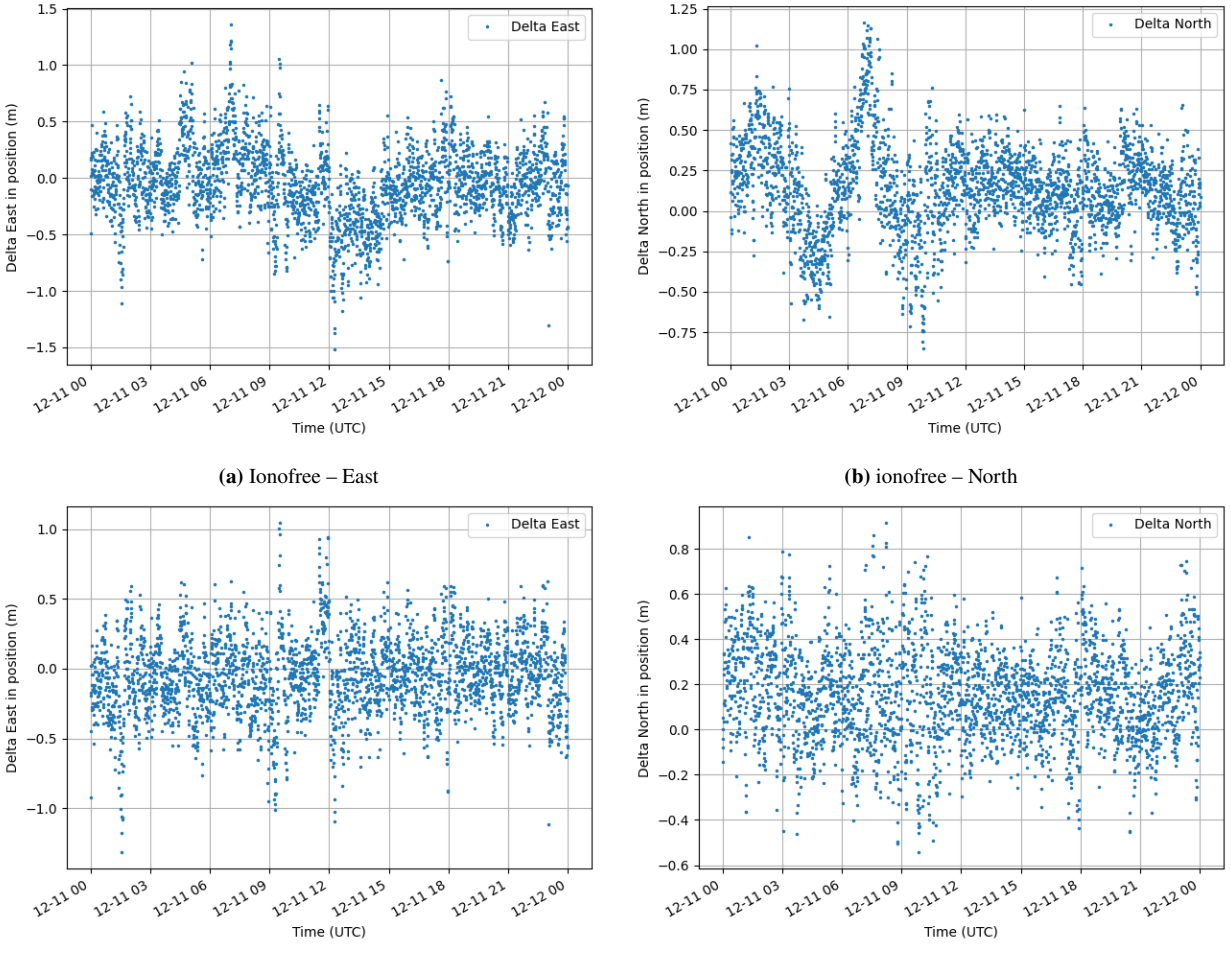

(a) Ionofree – East

(b) ionofree – North

(c) geometry with iono – East

(d) geometry with iono – North

Figure 2: Positioning errors of the KOUG station for the day 2023-345 in the east (left column) and north (right column) directions, in the case of a ionosphere-free estimation (first row) and the joint estimation of the geometry and the ionosphere delay (second row)

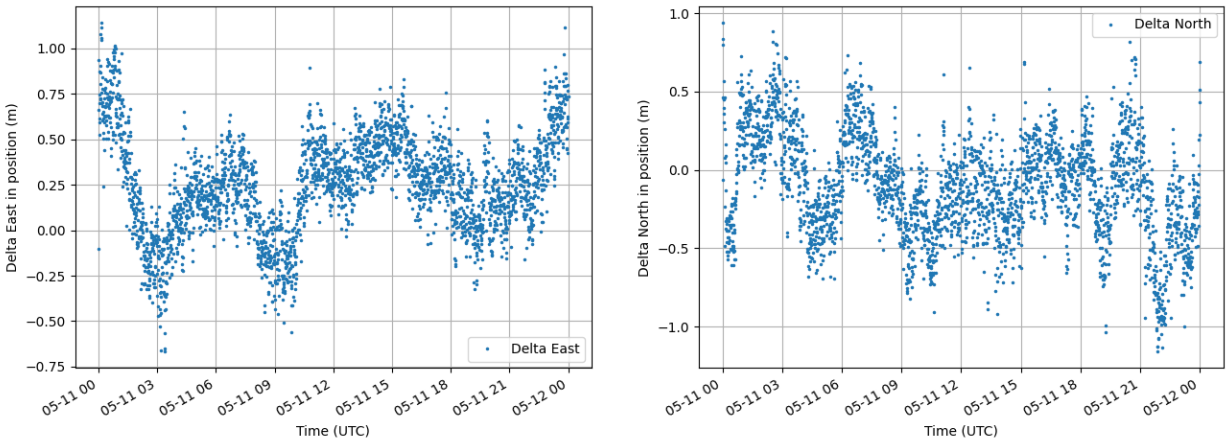

(a) Ionofree – East

(b) ionofree – North

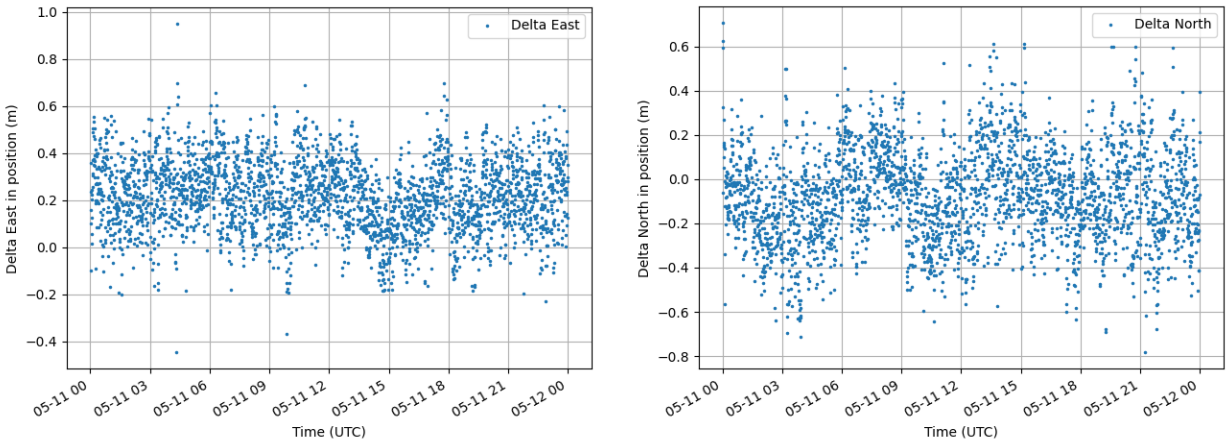

(c) geometry with iono – East

(d) geometry with iono – North

Figure 3: Positioning errors of the METG station for the day 2024-132 in the east (left column) and north (right column) directions, in the case of a ionosphere-free estimation (first row) and the joint estimation of the geometry and the ionosphere delay (second row)

V Impact of the ionosphere delay and its estimation on the generation of GNSS corrections

From 2015, CNES has set up a demonstrator called PPP-WIZARD (Precise Point Positioning With Integer Zero-difference Ambiguity Resolution Demonstrator) whose aim is to compute real-time corrections on GNSS satellites orbits and clocks, as well as code and phase biases, see Laurichesse (2011). To do so, measures gathered by around 160 reference ground stations are collected, and in particular the carrier phase measurements. The satellite phase biases can be computed only if the carrier-phase ambiguities of the measures from the ground station are resolved. Among them, the N1 ambiguity is the most difficult to solve for. Besides this, as explained in Gazzino et al. (2023), the ionosphere delay is part of the state vector, and its estimation is a by product of the GNSS corrections computation.

As it has been demonstrated in the previous section, the accuracy of the estimation process is highly dependant on the tuning of the Kalman filter, especially in case of high solar activity. This sensitivity in the parameters is reflected in the percentage of the time for which the N1 ambiguity is fixed. This section studies the link between the evolution of the Vertical Total Electron Content of the atmosphere and the percentage of N1 fixing. According to the reference Subirana et al. (2013), the total electron content is directly linked to the ionosphere delay. The Section I.2 demonstrated that the estimated ionospheric delay is always affected by code biases. Nevertheless, we are here interested in the variations of the TEC over several days. Since the code biases are almost constant, the conclusions of the analysis will still be correct.

The Figures 4 and 5 displays the evolution of the fixation rate of the GPS N1 ambiguity together with the estimated ionosphere delay for the TLSE station over several days, respectively for a low solar activity and a high solar activity. These figures exhibit a decrease in N1 fixation during the phase of increasing VTEC in the morning (upward slopes on the red curve), and an increase in the number of N1 fixations during the phase of decreasing VTEC in the late afternoon (downward slopes of the red curve). This means that the ionosphere delay evolution during a day affects the quality of the GNSS corrections generation.

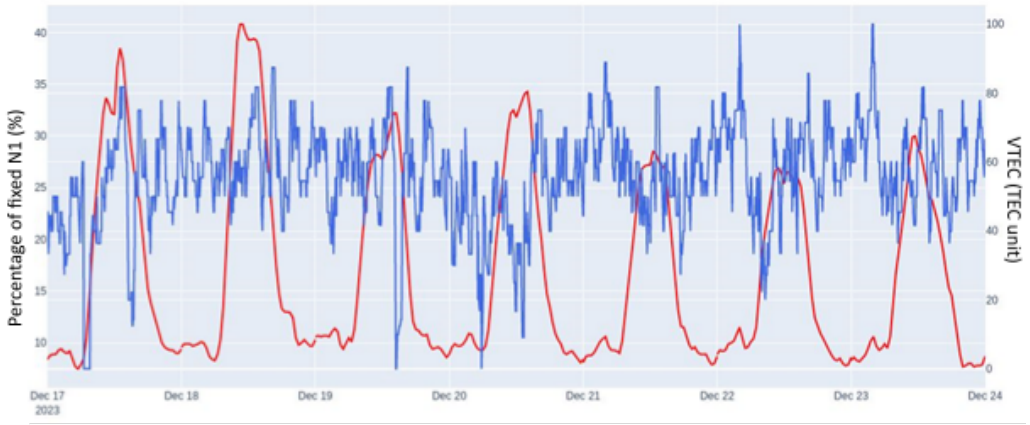

Figure 4: Evolution of the ratio of fixed N1 ambiguity (blue) and VTEC (red) for the TLSE station in December 2023.

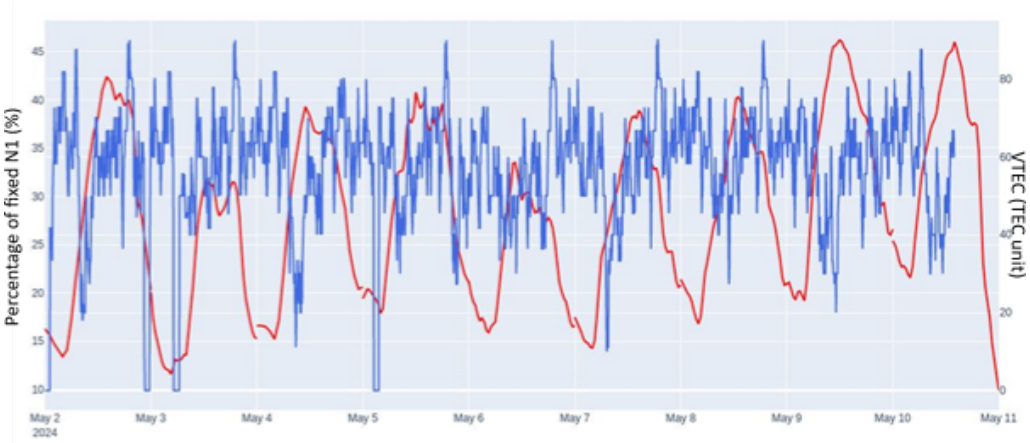

Figure 5: Evolution of the ratio of fixed N1 ambiguity (blue) and VTEC (red) for the TLSE station in May 2024.

VI Conclusion

The proposed receiver position estimation method attempts to take advantage of the multi-frequency context of today's Global Navigation Satellite Systems, either by extending the classical ionosphere-free combination to a noise-optimal multi-frequency one, or by including a term for the ionosphere delay of the visible satellites in the full ionosphere and geometry Kalman filter state vector. The proposed method has been applied for the positioning of ground stations, for days of low and high solar activities. The experiments have demonstrated that the positioning accuracy also depends on the intensity of the solar activity and the location of the station on the Earth. On top of that, the tuning of the Kalman filter process noises is decisive in order to decrease the positioning errors when compared to solutions computed with the classical ionosphere-free combination. The critical role played by the ionosphere delay is also applied in the more general framework of the GNSS corrections computation. A correlation between the decrease of the N1 fixation percentage and the increase of the TEC in the ionosphere has been demonstrated. All this tuning has been performed by hand. A next step will be to take into consideration higher order effect of the ionospheric delay and to apply more automatic adaptive Kalman filter techniques in order to further mitigate the ionosphere effect, especially in the years to come where the solar cycles may create intense space weather events.

REFERENCES

Chen, J. and Gao, Y. (2023). Real-time ionosphere prediction based on igs rapid products using long short-term memory deep learning. NAVIGATION: Journal of the Institute of Navigation, 70(2).

Gazzino, C., Blot, A., Bernadotte, E., Jayle, T., Laymand, M., Lelarge, N., Lacabanne, A., and Laurichesse, D. (2023). The cnes solutions for improving the positioning accuracy with post-processed phase biases, a snapshot mode, and high-frequency doppler measurements embedded in recent advances of the ppp-wizard demonstrator. Remote Sensing, 15(17):4231.

Gioia, C., Angrisano, A., and Gaglione, S. (2023). Galileo-based doppler shifts and time difference carrier phase: A static case demonstration. Sensors, 23(15):6828.

International GNSS Service (2020). IGS State Space Representation (SSR) Format. `https://files.igs.org/pub/data/format/igs_ssr_v1.pdf` visited on 2024-02-29.

Jakowski, N., Heise, S., Wehrenpfennig, A., Schlüter, S., and Reimer, R. (2002). Gps/glonass-based tec measurements as a contributor for space weather forecast. Journal of Atmospheric and Solar-Terrestrial Physics, 64(5-6):729–735.

Jazwinski, A. H. (2007). Stochastic processes and filtering theory. Courier Corporation.

Kaplan, E. D. and Hegarty, C. J. (2006). Understanding GPS - Principles and Applications, Second Edition. Artech House. Inc., MA.

Laurichesse, D. (2011). The cnes real-time ppp with undifferenced integer ambiguity resolution demonstrator. In Proceedings of the 24th International Technical Meeting of The Satellite Division of the Institute of Navigation (ION GNSS 2011), pages 654–662.

Odijk, D., Zhang, B., Khodabandeh, A., Odolinski, R., and Teunissen, P. J. (2016). On the estimability of parameters in undifferenced, uncombined gnss network and ppp-rtk user models by means of s-system theory. Journal of Geodesy, 90(1):15–44.

Subirana, J. S., Zornoza, J. J., and Hernandez-Pajares, M. (2013). Gnss data processing, vol. i: fundamentals and algorithms. ESA Communications, page 6.

Teunissen, P. J. and Montenbruck, O. (2017). Springer handbook of global navigation satellite systems, volume 10. Springer.

Wang, D., Zhang, S., Liu, T., Chen, Y., and Dong, Q. (2023). Performance analysis of cross-frequency doppler-assisted carrier phase tracking. GPS Solutions, 27(3):105.